Citation: Molecular Therapy — Methods & Clinical Development (2015) **2,** 15010; doi:10.1038/mtm.2015.10
© 2015 The American Society of Gene & Cell Therapy All rights reserved 2329-0501/15

www.nature.com/mtm

ARTICLE

Short-lived recombinant adeno-associated virus transgene expression in dystrophic muscle is associated with oxidative damage to transgene mRNA

Jean-Baptiste Dupont[1–3], Benoit Tournaire[1–3], Christophe Georger[4], Béatrice Marolleau[4], Laurence Jeanson-Leh[4], Mireille Ledevin[5], Pierre Lindenbaum[2,3,6], Emilie Lecomte[1–3], Benjamin Cogné[1–3], Laurence Dubreil[5], Thibaut Larcher[5], Bernard Gjata[4], Laetitia Van Wittenberghe[4], Caroline Le Guiner[1–4], Magalie Penaud-Budloo[1–3], Richard O Snyder[1,7,8], Philippe Moullier[1–3,7] and Adrien Léger[1–3]

Preclinical gene therapy strategies using recombinant adeno-associated virus (AAV) vectors in animal models of Duchenne muscular dystrophy have shown dramatic phenotype improvements, but long-lasting efficacy remains questionable. It is believed that in dystrophic muscles, transgene persistence is hampered, notably by the progressive loss of therapeutic vector genomes resulting from muscle fibers degeneration. Intracellular metabolic perturbations resulting from dystrophin deficiency could also be additional factors impacting on rAAV genomes and transgene mRNA molecular fate. In this study, we showed that rAAV genome loss is not the only cause of reduced transgene mRNA level and we assessed the contribution of transcriptional and post-transcriptional factors. We ruled out the implication of transgene silencing by epigenetic mechanisms and demonstrated that rAAV inhibition occurred mostly at the post-transcriptional level. Since Duchenne muscular dystrophy (DMD) physiopathology involves an elevated oxidative stress, we hypothesized that in dystrophic muscles, transgene mRNA could be damaged by oxidative stress. In the mouse and dog dystrophic models, we found that rAAV-derived mRNA oxidation was increased. Interestingly, when a high expression level of a therapeutic transgene is achieved, oxidation is less pronounced. These findings provide new insights into rAAV transductions in dystrophic muscles, which ultimately may help in the design of more effective clinical trials.

Molecular Therapy — Methods & Clinical Development (2015) **2**, 15010; doi:10.1038/mtm.2015.10; published online 8 April 2015

INTRODUCTION

Muscles of patients affected by muscular dystrophies suffer from profound metabolic disturbances. In Duchenne muscular dystrophy (DMD), the absence of Dystrophin leads to inflammation, rupture of calcium homeostasis, elevated oxidative stress, and eventually muscle fiber necrosis.[1] Ultimately, this leads to a progressive loss of ambulation and premature death.[1] In the last decade, successful gene therapy strategies have been designed in preclinical animal models of DMD using recombinant adeno-associated virus (rAAV) vectors.[2–4] However, one study evaluating rAAV-mediated gene transfer long-term reported a progressive reduction of therapeutic transgene expression attributed to the loss of vector genomes following muscle destruction as a result of subtherapeutic effect.[5] Additionally, in the DMD context other variables such as rAAV genome processing, transcriptional activity, and mRNA half-life have not yet been considered even though dystrophin-deficient muscles are characterized by: (i) a high level of DNA damage, which triggers DNA damage response (DDR) activation[6]; (ii) perturbations of the epigenetic landscape and the transcriptome[7,8]; and (iii) an elevated oxidative stress degrading cellular components.[9]

In this study, we injected dystrophic mdx4Cv mice and healthy C57BL6 (B6) controls intramuscularly with a nontherapeutic AAV8 vector expressing GFP and analyzed the transgene expression pattern at 15 and 60 days postinjection (pi). Our results indicate that GFP expression in dystrophin-deficient muscles is decreased at both protein and mRNA levels. However, we also demonstrated that the loss of rAAV genomes is not the only factor involved in this process. Indeed, rAAV transcriptional activity was found to be similar in B6 and mdx4Cv contexts, but the amount of vector transgene mRNA was reduced in mdx4Cv muscle in correlation with a higher level of mRNA oxidation. Importantly, this observation translated in the Golden Retriever muscular dystrophy (GRMD) dog muscle, upon gene therapy with a therapeutic rAAV vector. Transgene mRNA oxidation was however found reduced in muscles displaying high and sustained levels of transgene expression.

[1]INSERM UMR 1089/Atlantic gene therapies, Nantes, France; [2]University of Nantes, Nantes, France; [3]Nantes University Hospital, Nantes, France; [4]GENETHON, Evry, France; [5]UMR INRA ONIRIS 703/Atlantic gene therapies, Nantes, France; [6]INSERM UMR 1087/CNRS UMR 6291/L'Institut du Thorax, Nantes, France; [7]Department of Molecular Genetics and Microbiology, University of Florida College of Medicine, Gainesville, Florida, USA; [8]Center of Excellence for Regenerative Health Biotechnology, University of Florida College of Medicine, Gainesville, Florida, USA. Correspondence: A Léger (adrien.leger@inserm.fr) or P Moullier (moullier@ufl.edu)
Received 4 December 2014; accepted 17 February 2015

Our results emphasize the need to consider additional mechanisms when optimizing rAAV-mediated gene therapy. Transgene RNA stability is particularly sensitive to the modification of the cellular environment and thus deserves specific attention. Understanding the details and consequences of these molecular events paves the way for the design of improved gene therapy protocols for muscular dystrophies.

RESULTS

The level of rAAV-derived mRNA and protein is sharply reduced in murine dystrophic muscles

Six-week-old mdx4Cv and B6 mice received a serotype 2/8 rAAV-RSV-GFP vector (Figure 1) by bilateral intramuscular injection in the *tibialis anterior* (TA) muscle at a total dose of 4.0×10^{12} vg/kg. Muscle pathology was confirmed in mdx4Cv mice from the time of injection (6 weeks of age) to the end of the experimental protocol (14 weeks of age) exhibiting typical dystrophic features, including myofiber regeneration, membrane permeability, anisocytosis, and centronucleation (Supplementary Figure S1).

We quantified transgene GFP fluorescence intensity (arbitrary unit (a.u.)) on whole muscle cross-sections by slide scanning microscopy (Figure 2a,b). Consistent with previous reports, GFP intensity at 15 days pi in B6 muscles was hardly detectable (mean: 0.87 a.u.) but was strong at 60 days pi (mean: 77.9 a.u.). At this latter time-point, 4% of B6 muscle fibers showed intensities higher than 200 a.u. and 0.2% reached the maximal capacity of the detector (*i.e.*, signal saturation). In contrast, at 60 days pi, GFP fluorescence in mdx4Cv muscles remained low (mean: 4.8 a.u.) with 90% of the cells below 15 a.u. Therefore, comparing the two groups, the median GFP fluorescence intensity at 60 days pi was 16.2-fold lower in mdx4Cv than in B6 muscles. Quantification of transgene mRNA by reverse transcription (RT) quantitative polymerase chain reaction (qPCR) from muscle samples confirmed this observation. We found a 4.3-fold reduction of the GFP mRNA relative quantity (RQ) in mdx4Cv muscles at 15 days pi (median RQ: 0.69) compared with B6 (median RQ: 2.97), and 16.7-fold reduction at 60 days pi (median RQ for B6 mice: 5.02; mdx4Cv mice: 0.30; Figure 2c).

Altogether, these results indicate that the dystrophin-deficient muscle is an environment, in which rAAV-mediated GFP expression is hampered.

Vector genome loss is not sufficient to explain the reduced amount of transgene products in dystrophin-deficient muscles

A previous study in murine models of DMD[5] suggested that low transgene expression is the result of vector genome loss concomitant to muscle fiber degeneration. Similarly to mdx mice, mdx4Cv muscles show necrosis and regeneration (Supplementary Figure S1a). Therefore, we evaluated the vector genome persistence by qPCR. The reduction of the median vector genome per diploid genome (vg/dg) between 15 and 60 days pi was more pronounced in dystrophic muscles (from 1.65 to 0.19 vg/dg: 8.7-fold reduction, $P < 0.0001$) than in their healthy counterparts (from 2.96 to 1.46 vg/dg: 2.0-fold reduction, $P = 0.0089$) (Figure 3a). As a direct consequence, vg/dg ratios were significantly lower in mdx4Cv muscles compared to B6 controls at 15 days (1.65 versus 2.96 vg/dg, $P = 0.049$) and particularly at 60 days pi (0.19 versus 1.46 vg/dg, $P < 0.0001$).

We hypothesized that if vector genome loss observed in dystrophic mice is the only factor involved in the reduced transgene expression, then the mRNA per vg ratio should be similar between dystrophic and normal mice. We calculated the ratio of GFP mRNA RQ divided by rAAV vg/dg (abbreviated as RQ/vg), reflecting the ability of rAAV genomes to express detectable mRNA. The median RQ/vg ratio was found significantly lower in mdx4Cv than in B6 muscles at 15 days (RQ/vg = 0.31 versus 1.29, $P = 0.0019$) and 60 days pi (RQ/vg = 1.64 versus 4.28, $P = 0.0011$) (Figure 3b). These results indicate that rAAV genomes are not able to produce mRNA in mdx4Cv as efficiently as in healthy muscles and/or that transgene mRNA is less stable in the dystrophic muscle environment.

Epigenetic marks along the rAAV genomes are similar in healthy and dystrophin-deficient muscle

As previously shown, rAAV genomes persist in healthy muscles as chromatinized episomes devoid of DNA methylation, consistent with long-term transgene expression.[10,11] Since global chromatin patterns are deeply modified in DMD muscles,[7,8] we hypothesized that in mdx4Cv mice, rAAV genome expression may be downregulated at the transcriptional level by silencing epigenetic mechanisms. We focused our analysis on two well-described epigenetic modifications associated with silenced heterochromatin: Histone H3 Lysine 9 tri-methylation (H3K9me3) and DNA methylation on CpG dinucleotides.

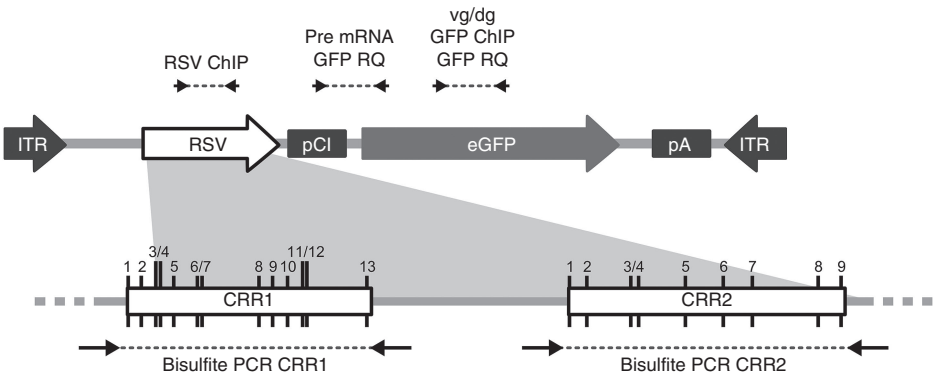

Figure 1 Schematic representation of the rAAV2/8-RSV-GFP genome and position of PCR primers. The expression cassette contains the complete Rous Sarcoma Virus (RSV) LTR promoter followed by an artificial pCI intron from the pCI plasmid backbone (Promega, Accession Number U47119), the GFP transgene, and the late poly-Adenylation signal from the SV40 virus. The bottom panel represents the two CpG Rich Region CRR1 and CRR2 identified in the RSV. CpG positions are marked by black vertical lines and numbered from 1 to 13 for CRR1, and from 1 to 9 for CRR2. Position of qPCR primers and bisulfite/PCR primers are represented above and below the figure, respectively.

© 2015 The American Society of Gene & Cell Therapy

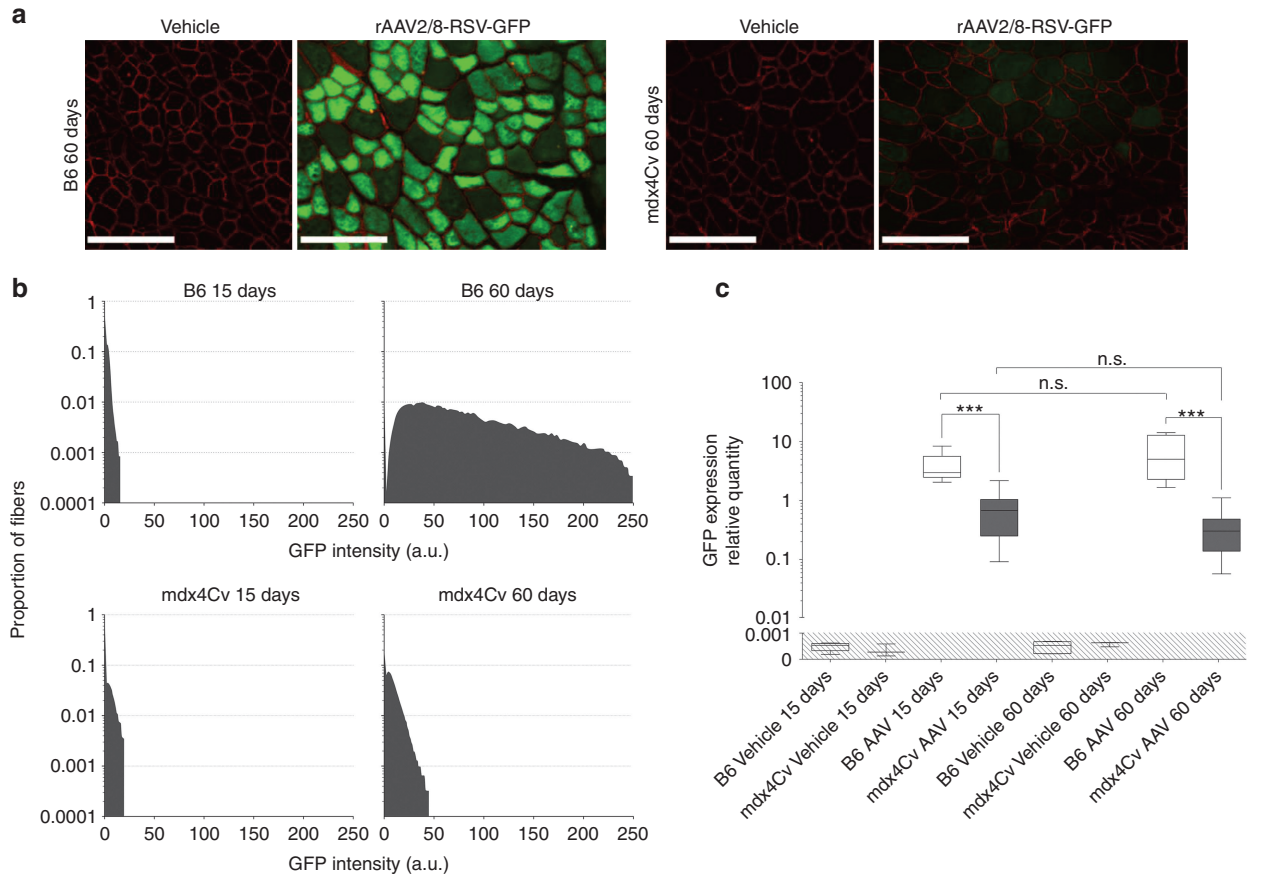

Figure 2 Evaluation of transgene expression in the muscle of recombinant adeno-associated virus (rAAV)-injected mice. mdx4Cv mice and C57BL/6J (B6) controls received bilateral intramuscular injection of an rAAV2/8-RSV-GFP vector (4×10^{12} vg/kg) or dPBS (Vehicle) in TA and were sacrificed 15 or 60 days postinjection. (**a**,**b**) GFP fluorescence on frozen muscle sections 60 days after AAV or vehicle injection. Whole muscle sections were stained with an anti-laminin antibody (red) and the GFP signal (green) was quantified in levels of grey (from 0 to 255 a.u.) on the entire section using a digital slide scanner and ImageJ software. (**a**) Representative panel. Scale bar = 200 µm. (**b**) Muscle fiber distribution according to GFP intensity, $n = 5$ mice per group. (**c**) Quantification of GFP expression in injected muscles by Taqman RT-qPCR normalized to the endogenous target Hprt. The data represent the median value (central line), the first and third quartiles (box) and first and ninth deciles (whiskers) of 10 mice per group. The shaded area delineates qPCR limit of detection. Statistics: Mann–Whitney's *U*-test. ***$P < 0.001$; n.s., non significant.

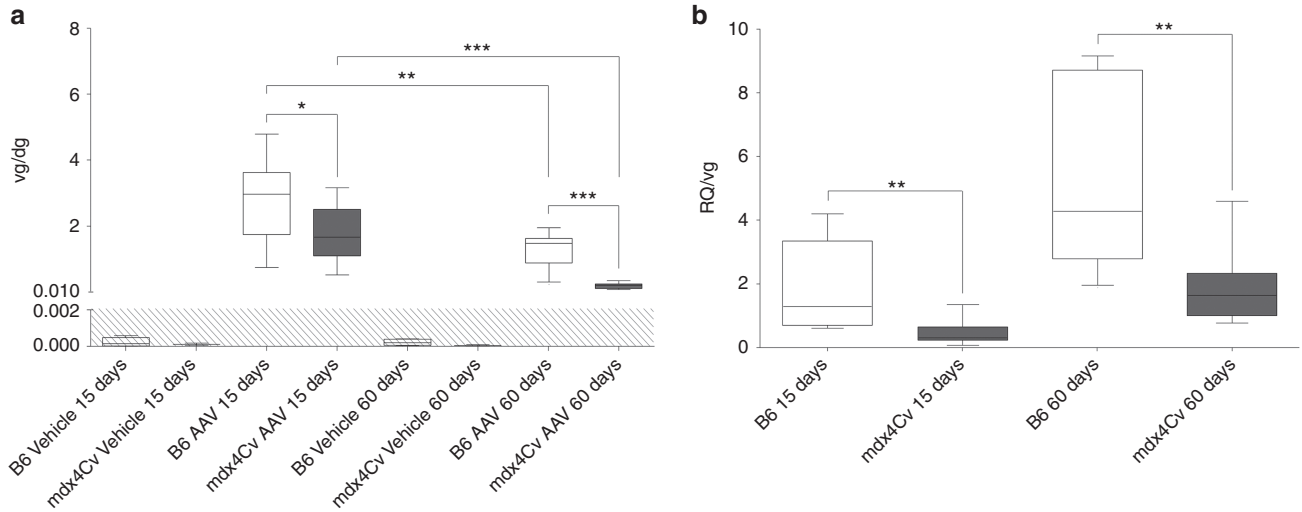

Figure 3 Persistence of AAV vector genome in dystrophic muscles and its implication on the reduction of transgene expression. mdx4Cv mice and C57BL/6J (B6) controls received bilateral intramuscular injection of an rAAV2/8-RSV-GFP vector (AAV, 4×10^{12} vg/kg) or dPBS (Vehicle) in TA and were sacrificed 15 or 60 days postinjection. (**a**) Quantification of AAV vector genome per diploid genome (vg/dg) by Taqman qPCR against GFP normalized with Albumin. (**b**) Plotting of individual ratios between GFP mRNA RQ and the AAV vg/dg copy number. The data represent the median value (central line), the first and third quartiles (box) and first and ninth deciles (whiskers) of 10 mice per group. The shaded area delineates qPCR limit of detection. Statistics: Mann–Whitney's *U*-test; *$P < 0.05$; **$P < 0.01$; ***$P < 0.001$; n.s., non significant.

© 2015 The American Society of Gene & Cell Therapy

Chromatin immunoprecipitation (ChIP) followed by qPCR indicated that similar levels of H3K9me3 decorated rAAV genomes isolated from mdx4Cv muscles or B6 controls (Figure 4a). Bisulfite conversion of muscle DNA and next-generation sequencing of two CpG-rich regions of the rAAV RSV promoter showed that methylation percentages were comprised between 0.6 and 5.4% (Figure 4b). While there was no significant difference at 15 days pi, each CpG position of RSV was methylated more frequently in mdx4Cv muscles than in B6 controls at 60 days pi. However, the difference never exceeded 1.65%, which is unlikely to have a notable impact on transcriptional rates (Figure 4b). Collectively, these data suggest that inhibition of rAAV genome transcriptional regulation by epigenetic mechanisms did not account for the differential amounts of GFP mRNA initially observed in mdx4Cv and healthy B6 mouse muscles.

The reduction of GFP mRNA level occurs at the post-transcriptional level

To confirm the absence of inhibition at the transcriptional level, we measured the transcriptional output of the RSV promoter in mdx4Cv muscles and B6 controls. Spliced RNAs are mainly cytosolic and their half-life depends on post-transcriptional mechanisms such as nonsense-mediated decay, No-Go decay or RNA interference.[12,13] By contrast, unspliced mRNAs are mainly nuclear and reflect more faithfully the raw transcriptional output of a given promoter. We included a chimeric intron—efficiently spliced *in vivo* (Supplementary Figure S2)—upstream of the GFP cDNA. While our previous RT-qPCR targeted both spliced and unspliced GFP mRNAs (RQ), we designed another RT-qPCR overlapping the chimeric intron to quantify specifically the unspliced GFP pre-mRNA fraction (pre-mRNA RQ). After normalization by vg/dg (later mentioned as pre-mRNA RQ/vg), here we observed no significant difference between mdx4Cv muscles and B6 controls notably at 60 days pi where the median and range values were similar (Figure 4c, median = 0.078 and range = 0.044–0.150 for mdx4Cv mice; median = 0.078 and range = 0.036–0.154 for B6 controls). These data indicate similar transcriptional outputs and pre-mRNA regulations of rAAV genomes in healthy and dystrophin-deficient murine muscles. We concluded that the lower GFP RQ values measured in mdx4Cv mice result from post-transcriptional events impacting on GFP mRNA half-life in the cytoplasm.

Oxidation of the GFP transgene mRNA is higher in mdx4Cv muscles

To further understand mechanisms at stake in reducing cytoplasmic spliced GFP mRNA quantities, we hypothesized that mRNA metabolism could be disturbed by reactive oxygen species leading to reduced stability. This hypothesis would be consistent with the increased oxidative stress described in muscles of DMD patients and mdx mice.[9,14–16] RNA oxidation occurs most frequently on Guanine nucleotides resulting in 8-HydroxyGuanine (8-HOG), which can be detected by antibody-based techniques. First, we used an

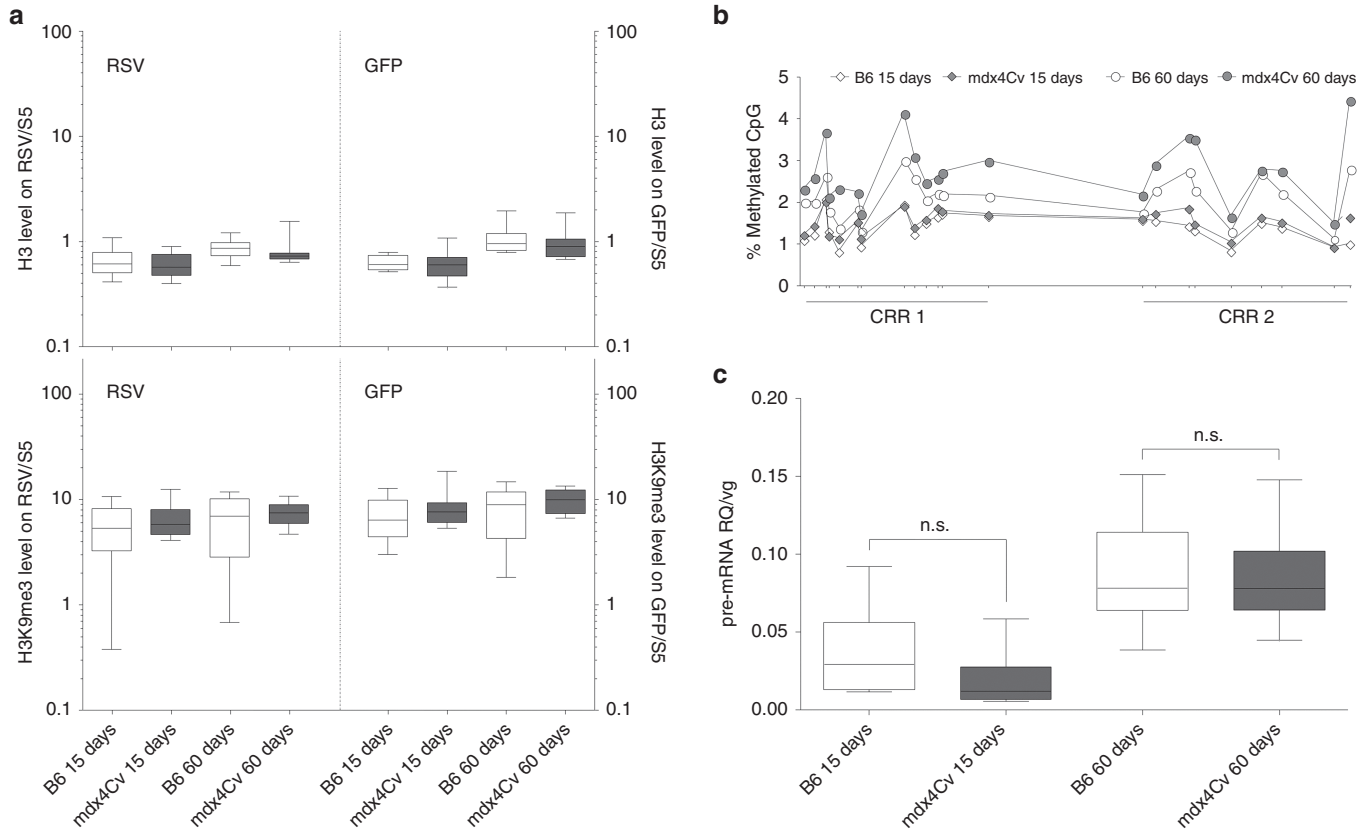

Figure 4 Regulation of transgene expression at the transcriptional and post-transcriptional level. mdx4Cv mice and C57BL/6J (B6) controls injected intramuscularly with an AAV8-RSV-GFP vector (4×10^{12} vg/kg) in TA were sacrificed 15 or 60 days postinjection. (**a**) Immunoprecipitation of muscle chromatin using anti-H3 (top) and anti-H3K9me3 (bottom) antibodies followed by qPCR targeting RSV (left) and GFP (right). Data were normalized with the endogenous mouse heterochromatin segment Satellite-5 (S5). (**b**) DNA methylation assessment on two CpG-Rich Regions (CRR) of RSV by bisulfite conversion and next-generation sequencing. Data are represented as % of methylation for each CpG position along RSV. The distance between the CpG was adjusted to reflect the real positions on a linear DNA molecule. (**c**) Quantification of AAV genome transcriptional activity by RT-qPCR against unspliced GFP mRNA and normalization by vg/dg (pre-mRNA RQ/vg). (**a**,**c**) Graphic representation is as follows: median value (central line), the first and third quartiles (box) and first and ninth deciles (whiskers) of 10 mice per group. Statistics: Mann–Whitney's *U*-test; n.s., nonsignificant.

© 2015 The American Society of Gene & Cell Therapy

enzyme-linked immunosorbent assay to quantify the overall level of 8-HOG in total RNA extracted from injected muscles. At 60 days pi, there was a higher RNA oxidation in mdx4Cv muscles (median = 14.4, range = 13.6–16.3) compared with B6 controls (median = 13.9, range = 12.6–15.6), but the difference was not significant. Therefore, RNA oxidation, if involved, is not a widespread phenomenon but may rather be restricted to specific RNA subpopulations.

To analyze selected RNA, the oxidized RNA fraction was extracted from the whole RNA INPUT using a RNA Immunoprecipitation (RNA IP) protocol with an anti-8-HOG antibody. We designed a RT-qPCR assay targeting three different mRNA, either with a ubiquitous (Hprt and Gapdh) or a muscle-restricted (Myoglobin) expression. The relative abundance of each target was determined in both INPUT and immuno-precipitated fractions, and results were expressed as a percentage of INPUT. In B6 muscle RNA obtained 60 days pi, %INPUT for the three mRNAs were found to be similar (Hprt: 4.5–9.6%, Gapdh: 12.0–15.65%, Myoglobin: 4.2–11.6%), suggesting the existence of a basal oxidation level in healthy mouse muscles. In contrast, there was a selective hyperoxidation in mdx4Cv muscles 60 days pi affecting Hprt (12.8–20.7%, $P = 0.012$) and Gapdh (19.8–37.0%, $P = 0.006$) mRNA, but not Myoglobin (5.5–10.4%, n.s.) (Supplementary Figure S3). When applied to GFP transgene mRNA in B6 and mdx4Cv muscles, we found oxidized mRNA within the range of the three endogenous mRNAs (5–10%) and significantly higher values, ranging from 12.5 to 37.5% ($P = 0.006$) (Figure 5a), respectively.

In conclusion, significant oxidative damage to GFP transgene mRNA occurs in dystrophic muscles and correlates with lower cytoplasmic mRNA levels. Ultimately, this phenomenon might be responsible, to some extent, for the low GFP signal found in mdx4Cv muscles.

High expression of a therapeutic transgene is correlated with a lower rAAV mRNA oxidation in dystrophin-deficient dog muscles

To further correlate the relationship between the mRNA oxidation status and the expression of the transgene, we measured the level of transgene mRNA oxidation in a unique context where four GRMD dogs were injected locoregionally in one entire forelimb[4] with an rAAV8 vector expressing a truncated but functional form of dystrophin (µDys). µDys sarcolemmal localization was confirmed by immunofluorescence on transduced muscle sections with variable ratios of µDys-expressing fibers among the 19 muscle samples analyzed 13–16 weeks pi (Le Guiner *et al.*, manuscript in preparation). We also measured the expression of µDys at the mRNA level by RT-qPCR and distinguished two categories of samples: samples with low transgene expression (RQ < 1) as opposed to samples with high transgene expression (RQ > 2). Starting from the same RNA INPUTs, we applied the RNA IP protocol and subsequent RT-qPCR in order to assess the µDys mRNA oxidation status. In samples with low µDys RQ (RQ µDys < 1), transgene mRNA oxidation (µDys %INPUT) ranged between 9.38 and 24.81% with a median of 19.25%, which was comparable to the results obtained for non-therapeutic GFP mRNA in mdx4Cv mice (Figure 5b). Remarkably, in muscle samples with high therapeutic transgene expression levels (RQ µDys > 2), RNA oxidation was reduced to a median value of 7.23% and only one sample had a %INPUT above 10% (Figure 5b). Similarly to the results described previously in mdx4Cv mice, transgene mRNAs are susceptible to oxidation in GRMD muscles when the mRNA is expressed below the therapeutic threshold. In contrast, high transgene expression, believed to be equal or above the therapeutic threshold, results in basal values of transgene RNA oxidation similar to healthy murine muscle samples.

Altogether, this study highlights novel mechanisms restricting rAAV transduction efficiency in dystrophic muscles. More than the physical loss of vector genome due to the progressive degeneration of dystrophic muscle cells, our data indicate that oxidative damage to transgene mRNA is also an important factor to consider, which in turn emphasizes the need to determine the therapeutic threshold in complex diseases.

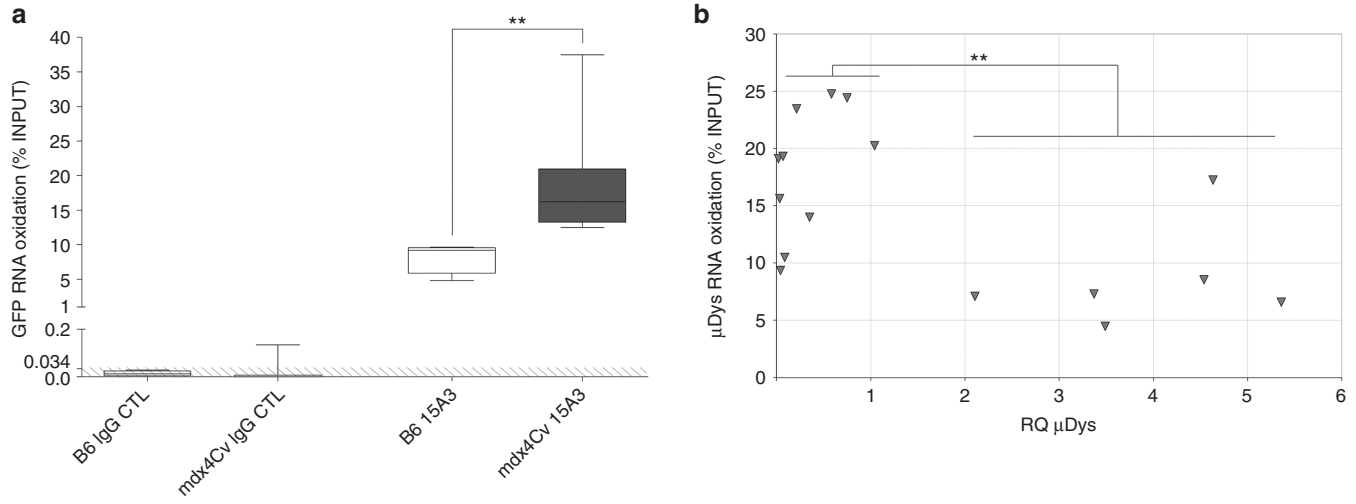

Figure 5 Transgene mRNA oxidation after rAAV injection in dystrophic mice and dogs. (**a**) RNA Immunoprecipitation analysis of GFP mRNA oxidation at 60 days postinjection in the TA muscles of mdx4Cv mice and C57BL/6J (B6) controls, using a specific anti-8-HOG antibody (15A3). No background signal was obtained with the isotype control (IgG CTL). The GFP mRNA copy number was measured by RT-qPCR after Immunoprecipitation and expressed as a percentage of INPUT. The data represent the median value (central line), the first and third quartiles (box) and first and ninth deciles (whiskers) of four (B6) or seven (mdx4Cv) mice per group. The shaded area delineates qPCR limit of detection. Statistics: Mann–Whitney's *U*-test; $^{**}P < 0.01$. (**b**) Microdystrophin (µDys) mRNA oxidation after rAAV8 locoregional injection in Golden Retriever muscular dystrophy (GRMD) dogs. % INPUT were obtained with the same protocol as in **a** and plotted as a function of µDys RQ, measured by RT-qPCR and normalized with the endogenous target Rpl32. The 19 samples represent various forelimb muscles collected from four GRMD dogs injected with a similar vector dose (1×10^{13} vg/kg) and euthanized between 13 and 16 weeks postinjection. Statistics: Mann–Whitney's *U*-test between two distinct categories of samples (RQ < 1 versus RQ > 2); $^{**}P < 0.01$.

© 2015 The American Society of Gene & Cell Therapy

DISCUSSION

In this study, we showed that the pathophysiological status of a diseased organ can impact dramatically on rAAV-mediated gene expression. Here, in the absence of a strategy based on pretreating the tissue prior to rAAV administration, the dystrophic muscle environment impairs optimal gene expression precluding the potential for therapeutic efficacy.

Our central observation using a nontherapeutic transgene is the lower level of GFP mRNA in dystrophic muscles despite the use of a strong and constitutive promoter in the vector (RSV),[11,17] resulting in low GFP fluorescence *in vivo* both at early (15 days) and later (60 days) times pi. Of note, the reduction of fluorescence in mdx4Cv strictly parallels the reduction of GFP mRNA (16-fold decrease), which led us to explore restriction factors occurring at the pretranslation level. Lower transgene mRNA levels in mdx4Cv muscles were partially correlated with the reduced persistence of the rAAV vector genomes, consistent with previous studies conducted in other murine models of muscular dystrophies such as the mdx/utr-/- double knock-out mouse[5] or the α-sarcoglycan (sgca)-deficient mouse.[18]

In addition to vector genome clearance occurring in degenerative muscle, rAAV transduction may also be hampered at others steps such as genome processing, transcriptional activity, mRNA stability, or production of transgenic proteins. We investigated beyond the contribution of vector genome loss and used the RQ/vg ratio that we defined as the efficiency of comparable rAAV genome populations to produce and maintain stable GFP mRNA molecules. Similar RQ/vg values between mdx4Cv and B6 mice would have meant that vector genome clearance was the only cause explaining rAAV restriction in dystrophic muscles. In this study, however, RQ/vg ratios were found significantly lower in mdx4Cv mice, suggesting that an additional mechanism(s) is responsible for lower vector-derived mRNA levels.

The first steps following nuclear entry include second-strand synthesis and genome rearrangements into concatemeric or circular forms. These molecular events are controlled by numerous proteins notably involved in endogenous DDR.[19,20] Recent studies highlighted that cellular permissivity to rAAV transduction is inhibited by DDR proteins such as members of the Mre11-Rad50-Nbs1 (MRN) complex or Atm.[19–22] Even if these proteins are mostly regulated post-translationaly, their overexpression was recently linked with lower rAAV efficiency.[21] Therefore, we monitored by RT-qPCR the expression of several DDR genes (Mre11, Rad50, Nbs1, Atm, Atr, DNA-PKc) in our mdx4Cv and B6 muscle samples. All of them were found significantly overexpressed ($P < 0.01$) in mdx4Cv muscles (Supplementary Figure S4) and might therefore inhibit rAAV genome processing into productive molecular forms. Even if an unbalanced DDR pathway could have been an additional disease-related restriction, it was not further considered in this study as we demonstrated that pretranscriptional mechanisms are unlikely to be involved.

One obvious parameter susceptible to inhibit rAAV genome expression in mdx4Cv muscles could have been epigenetic silencing. We previously showed that circular rAAV genomes associate with cellular histones *in vivo* to form episomal chromatin structures, suggesting the possibility of epigenetic regulation.[10] Our previous study showed a hypomethylation of CpG along the RSV promoter in healthy nonhuman primate muscle and liver explaining the long-term transgene expression in healthy tissues.[11] In the context of DMD, several investigators have described the deregulation of epigenetic enzymes such as DNA Methyltransferases following inflammation and cytokine secretion[23] or Histone Deacetylases specifically in the muscle of mdx mice or DMD patients.[7,8] We focused on two marks known to be coenriched at constitutive heterochromatin loci: high CpG methylation of promoters and the histone lysine methylation H3K9me3. While our results did not show a repressive epigenetic pattern along rAAV genome in dystrophic muscles, we cannot exclude other transcription regulatory mechanisms. Of note, we found an unusual epigenetic pattern in all samples (mdx4Cv and B6) where rAAV genomes were essentially devoid of DNA methylation along the RSV promoter and enriched in H3K9me3. In addition to its role in gene silencing, H3K9me3 seems to be involved in DNA double strand break early signaling.[24,25] As rAAV genome undergoes extensive rearrangements at early steps post nuclear entry, this unusual pattern may be the result of conflicting signals between DNA repair and transcription.

In order to assess transgene expression efficiency more faithfully, we measured the ability of rAAV genome to produce GFP pre-mRNA. We considered only the unspliced fraction produced by equivalent vector genome populations and found similar transcriptional activities for rAAV genomes in mdx4Cv muscles and B6 controls, indicating that the reduction of GFP mRNA levels observed initially is the result of post-transcriptional events.

In the absence of dystrophin, myocytes endure a variety of molecular perturbations leading to inflammation, rupture of calcium homeostasis and oxidative stress. Once mature mRNAs leave the nuclear environment where exported into the cytoplasm, they become exposed to these stresses and to RNA quality control systems (nonsense-mediated decay, No-Go Decay, RNA interference[12,13]). Among them, oxidative stress seemed particularly relevant in the context of DMD patients and mdx mice. In the absence of dystrophin, the level of reactive oxygen species is increased in muscles and leads to the oxidation of membrane lipids, proteins, or DNA.[9,15,16] To our knowledge, however, the oxidation of RNA was never described in any animal model of DMD and the only report in the context of muscle diseases concerns patients suffering from myopathies with rimmed vacuoles.[26] Nevertheless numerous studies already described RNA oxidation and demonstrated its direct implication in the physiopathology of age-associated disorders including Alzheimer and Parkinson disease, dementia, or muscle atrophy.[27,28] Mechanistically, RNA oxidation by Guanine hydroxylation can result in strand scission[29] and leads to translation errors by ribosome stalling[30,31] which in turn activates RNA No-go decay.[12] We described a higher level of oxidation not only on transgene mRNA but also on several endogenous targets in mdx4Cv muscles. In GRMD muscle samples, we also demonstrated that rAAV-derived mRNA is highly oxidized when the expression of the therapeutic transgene is low. However, one of the mRNA targets examined in mice (Myoglobin, Supplementary Figure S3) and additional targets in GRMD dogs (Rpl32, Gusb, data not shown) seemed unaffected by oxidative stress. This indicates that mRNA oxidation in dystrophic muscles may be a selective process, as it was previously described *in vitro*-induced oxidative stress,[31,32] as well as *in vivo* in a mouse model of amyotrophic lateral sclerosis[33] or in postmortem brain samples from Alzheimer patients.[27] The factors explaining this selectivity are currently unknown but may include differential RNA motifs or folding, as well as intracellular localization. The basal expression level of the gene does not seem to have an influence, since in our study two promoters (Myoglobin and RSV) leading to similar expression levels did not result in similar mRNA oxidation levels.

Our results obtained in two animal models of DMD with two different rAAV products (GFP and μDys) suggest that mRNAs derived from rAAV vectors are particularly sensitive to oxidative damage caused by free radicals in dystrophic muscles. This is likely to result in the lower efficiency of rAAV in combination with other

© 2015 The American Society of Gene & Cell Therapy

parameters such as the faster clearance of vector genome due to fiber degeneration. However, encouraging results in GRMD muscle samples showed that the high expression of µDys was able to significantly reduce the relative proportion of oxidized mRNA. This gives further credit to the "threshold hypothesis" suggesting that a critical dose of therapeutic vector has to be reached to restore muscle fiber integrity and allow the persistence of rAAV genome expression in the long-term.

While current protocols rely on the injection of elevated rAAV doses, understanding how the dystrophic muscle context and the related pathophysiological factors are affecting rAAV vector efficiency might accelerate the emergence of alternative strategies. Among these strategies, developing dedicated protocols, such as pretreating the tissue with antioxidant prior to vector administration, may improve rAAV therapeutic index in future trials for DMD.

MATERIALS AND METHODS

Quality assurance

Quality management system has been implemented to cover all activities in INSERM UMR 1089 laboratory including the management of research teams and production of research-grade viral vectors. This system has been approved by Lloyd's Register Quality Assurance to meet requirements of international Management System Standards ISO 9001:2008.

Production of rAAV vectors

The pAAV-RSV-GFP-pA vector plasmid contains the Rous Sarcoma Virus promoter (RSV), followed by a short synthetic intron (pCI plasmid, Promega, Madison, WI), the enhanced green fluorescent protein (GFP) coding sequence and the late SV40 polyadenylation (pA) signal. The expression cassette was cloned between AAV2 inverted terminal repeats (ITR) (Figure 1). Research grade single-stranded (ss) AAV 2/8 vectors were produced by the INSERM UMR 1089 vector core. Briefly, HEK293 were transfected with the pAAV-RSV-GFP-pA vector plasmid together with helper plasmid pDP8 (which contains AAV2 rep, AAV8 cap, and adenovirus helper genes). Cells were harvested 48–72 hours post-transfection and centrifuged at low speed, then the rAAV8 particles contained in the supernatant were purified by double cesium chloride gradient ultracentrifugation followed by dialysis against Dulbecco's phosphate-buffered saline (Lonza, Verviers, Belgium). Vector genomes and infectious particles (ip) were quantified by Dot Blot and Replication Center Assay respectively. The vector titers were 1.2×10^{13} vg/ml and 2.4×10^{9} ip/ml. Detection of Rep-ITR junctions in the final product did not reach the limit of quantification by qPCR.

Ethic statement and animal experimentation

Generation of genetically modified mice by rAAV vectors was authorized by the French ministry of research (#5833) and all experimental procedures were validated by the Departmental Direction of Veterinary Services (#A44-124) in accordance with the French law on vertebrate laboratory animal experimentation (Decree 87-848, 1987). All animals were handled following guidelines for the Care and Use of Laboratory Animals. Mouse experiments were conducted in SPF grade animal facilities based in Nantes university (UTE IRS-UN, Nantes, France) and Genethon (Evry, France) after approval by the research ethics boards from Loire Atlantique (#CEEA.2011.18) and from Genethon (#CE 11-05).

Five- to 7-week-old SPF-grade C57BL/6J (Charles River, Wilmington, MA) and mdx4Cv (B6Ros.Cg-Dmd$^{mdx\text{-}4Cv}$/J, in-house breeding) mice were randomly assigned to receive in each *tibialis anterior* (TA) muscle either dPBS or 5.0×10^{10} vg of the ssAAV2/8-RSV-GFP-pA vector diluted in dPBS, for a total dose of 4.0×10^{12} vg/kg. Prior to injection, mice were anesthetized by a single intraperitoneal administration of Ketamine/Xylazine. Animals were euthanized at 15 or 60 days postinjection by exsanguination under a high dosage isoflurane inhalation anesthesia. For each animal, whole injected muscles, noninjected muscles, liver, lymphoid organs, and sera were collected and processed within 10 minutes, as follows: samples for molecular biology analyses were sliced in pieces of 1–2 cubic mm, randomly distributed in Eppendorf tubes and snap-frozen in liquid nitrogen before long-term storage at −80 °C; samples for histology were placed in disposable base molds and embedded in Tissue-Tek optimum cutting temperature (OCT) compound (Sakura, Torrance, CA). Molds were subsequently frozen for 1 minute in cold isopentane and stored at −80 °C.

Quantitative analyses of GFP expression by slide scanning microscopy

Skeletal muscle cryosections (5 µm) were collected on slides, air dried, fixed with 4% PFA pH7.4 for 10 minutes, and permeabilized 10 minutes in 0.3% Triton X100 (Sigma-Aldrich, St. Louis, MO). Saturation was performed in 10% goat serum (Dako X090710, Troy, MI) for 30 minutes at room temperature (RT). Then, slides were incubated with the anti-mouse laminin primary antibody at 1:100 (rat monoclonal antibody MAB1905, Chemicon, Temecula, CA), for 1 hour at 37 °C. After washing with PBS, sections were incubated for 1 hour at RT with the Alexa fluor 555-conjugated anti-rat antibody at 1:400 (goat IgG A21434 from Invitrogen, Life Technologies, Carlsbad, CA). Nuclei were stained for 15 minutes at RT with DRAQ5 (DR500200, Biostatus limited, Shepshed, UK) at 1:1,000. Finally, slides were mounted with Prolong Gold (Invitrogen, P36934). To quantify GFP fluorescence, muscle sections were scanned using a Digital slide scanner (Nanozoomer 2.0, Hamamtsu, Japan) using FITC and TRITC filters to detect GFP and laminin respectively. For each group, exposure times were set up so that no GFP fluorescence would be detected on dPBS-injected sections. Myofibers were individualized using laminin fluorescence. The total number of fibers including GFP negative fibers and the mean GFP intensity of each cell were determined using ImageJ software on a gray scale ranging from 0 to 255 a.u. (Rasband, W.S) (ImageJ, US National Institutes of Health, Bethesda, MD, http://imagej.nih.gov/ij/, 1997-2012).

Nucleic acid extraction and reverse transcription

Genomic DNA was extracted from 50 to 100 mg of muscle and liver samples using Gentra Puregene Blood Kit (Qiagen, Venlo, Netherlands). Briefly, frozen tissues were disrupted in Cell Lysis Solution using the Qiagen Tissue Lyser II (30 seconds at 30 Hz). DNA was then recovered according to the manufacturer's instructions and stored at −20 °C. DNA concentration and purity were evaluated by microliter optical density (ratio A260 nm/A280 nm between 1.8 and 2). Total muscle RNA was obtained from frozen tissue samples by mechanical disruption (Tissue Lyser II: 2×30 seconds at 30 Hz), organic extraction using TRI Reagent (Ambion, Life Technologies, Carlsbad, CA)/chloroform (Sigma-Aldrich) purification and isopropanol precipitation (Carlo-Erba, Milan, Italy). RNA samples were stored at −80 °C until further use. Contaminating DNA was eliminated by two successive digestions with DNAse (TURBO DNA-free kit, Ambion). DNase-treated RNA was subsequently reverse transcribed with poly-dT primers and M-MLV Reverse-Transcriptase (Invitrogen) following the manufacturer's instructions and cDNAs were stored at −20 °C before analysis. Control samples without Reverse-Transcriptase were also prepared in order to verify the absence of DNA contaminants. For all samples, DNA contamination was not detected by qPCR.

In situ chromatin immunoprecipitation

The ChIP protocol was adapted from standard procedures for the study of murine muscle chromatin. Briefly, muscles were pulverized under liquid nitrogen using mortar and pestle. The resulting powder was incubated in 1% formaldehyde to cross-link DNA and proteins and the nuclei were then isolated by chemical and mechanical extraction. Following chromatin sonication (to an average size of 250–350 bp), IP was performed with the appropriate antibody (anti-H3: ab1791 from abcam, Cambridge, UK; anti-H3K9me3: abcam ab8898). Finally, Bound and Unbound DNA were purified separately and analyzed by qPCR. A detailed description of the different steps is provided in the Supplementary Material section.

Bisulfite conversion and Illumina Miseq sequencing

DNA methylation was quantified using the Methyl Detector kit (Active motif, Carlsbad, CA) for bisulfite conversion and PCR amplifications (Supplementary Table S1) of two CG rich regions (Figure 1, CRR1/2) were performed. Subsequently, C/T polymorphisms were quantified by illumina Miseq deep sequencing. A count of the methylated bases was performed using a custom program implementing an alignment algorithm handling degenerate bases. The C++ code is freely available at the following URL: http://variationtoolkit.googlecode.com/svn/trunk/src/methyl01.cpp.

RNA immunoprecipitation

RNA inputs (1.5 µg of DNAse-treated RNA) were distributed by B.T. in Nonstick RNAse-free tubes (Ambion). The following steps including data analysis were conducted blindly by J.B.D. First, samples were incubated at RT for 4 hours

© 2015 The American Society of Gene & Cell Therapy

with the anti-8-hydroxyguanine (8-HOG) 15A3 antibody (abcam ab62623) or with an IgG2b isotype control (Thermo Fisher, Waltham, MA) diluted in RNA IP buffer (25 mmol/l Tris pH7.4, 150 mmol/l KCl, 5 mmol/l EDTA, 0.5 mmol/l DTT, 0.5% Igepal, 100 U/ml RNAseOUT inhibitor (Invitrogen), supplemented with Complete EDTA-free protease inhibitor (Roche, Basel, Switzerland)). Precipitation was performed O/N at 4 °C after addition of protein A magnetic beads (Dynabeads-ProteinA, Life Technologies) with gentle rotation. RNA bound to the beads was then washed five times in PBS 0.04% Igepal, eluted with PBS 0.04% Igepal, 1% SDS, 0.08 mg/ml proteinase K and incubated at 55 °C for 30 minutes with regular vortex. The BOUND RNA was collected in clean tubes, purified with proteinase K and isopropanol precipitation. RNA pellets were washed in ethanol 80%, dried, resuspended in RNAse-free water, and finally stored at −80 °C until further use. After titration, the reverse transcription reaction was performed on 250 ng RNA with the RT² First Strand Kit (Qiagen) following the manufacturer's guidelines for small samples.

Quantitative PCR

Since most of our results relied on qPCR analyses, we followed MIQE recommendations[34] and reported comprehensively our controls and validation checkpoints in the following paragraphs. Characteristics of targets and oligonucleotides are listed in Supplementary Table S1. Primers and probes were provided by Sigma after purification by a desalting procedure, except those already included in kits (Reference Gene Panel Mouse, TATAA Biocenter, Gothenburg, Sweden). Quantitative PCR reactions were performed in a final volume of 20 µl from either 50 ng of DNA or 2.5 µl of 10-fold diluted cDNA. All samples were analyzed in duplicates by StepOne Plus thermal cycler (Applied Biosystem). The predicted specificity of qPCR reactions was verified by UCSC *in silico* PCR (http://genome.ucsc.edu/cgi-bin/hgPcr). For SYBR green-based qPCR we also systematically validated the specificity by melting curve analysis. Quantification cycle (C_q) values were calculated with StepOne software v2.3 using automatic baseline and a threshold fixed manually for each assay (Supplementary Table S1). DNA copy numbers were inferred by calibration curve quantitation established with serial dilutions of linearized plasmids containing the target sequences. Exclusion conditions including r^2, amplification efficiency, and linear dynamic range are listed in Supplementary Table S1. The different parameters analyzed in this study were obtained as follows: (i) for the determination of vector genome copy number (vg) per host diploid genome (dg) the mouse Albumin (mAlb) was selected as reference gene (vg/dg: 2 × GFP copy number/mAlb copy number); (ii) for RT-qPCR analyses of GFP (RQ and RQ'), the reference gene was determined using the Reference Gene Panel Mouse (TATAA Biocenter). Twelve murine reference transcripts were analyzed; data were compared with NormFinder and GeNorm algorithms and Hypoxanthine-guanine phosphoribosyltransferase (Hprt) was selected as presenting the lowest variations between the analyzed tissues. RQ and RQ' were calculated with the 2-ΔCq method (RQ = 2-(C_q target − C_q Hprt)) in the case of similar efficiencies between target and HPRT qPCR reactions. If the efficiencies were different, this calculation was adapted as follows: RQ = ((EHprt) × (C_q Hprt))/((Etarget) × (C_q target)), as previously described[35]; (iii) ChIP qPCR data were normalized using the Satellite-5 control target, which is comprised in a single copy LINE/LTR located in a murine gene and which was found particularly enriched in H3K9me3. ChIP relative enrichment was calculated from qPCR data as follows: Bound/(Bound+Unbound) for target sequences (RSV or GFP) divided by B/(B+U) obtained for Satellite-5; (iv) percentages of INPUT obtained after RNA IP were calculated from qPCR data by dividing the copy number of the desired target in the isolated fraction by the copy number of the same target in the INPUT. In each case, sensitivity thresholds were calculated using the smallest amount of plasmid template detected in calibration curves and the average copy number of reference gene measured by the appropriate qPCR.

General data handling and statistical analysis

Data were processed using PRISM 5 software (GraphPad, La Jolla, CA). Most of the graphics were represented as "box and whiskers" plots, with the median value of the sample indicated as a line inside the box; box extremities: first to third quartiles; whiskers extremities: first to ninth deciles. Due to the small sample sizes (maximum 10 mice per separate group), data were analyzed using only the nonparametric Mann–Whitney *U*-test.

ACKNOWLEDGMENTS

This work was supported by the Region Pays de la Loire and the Association Francaise contre les Myopathies (AFM). The authors would like to thank Marine Allais, the Atlantic Gene Therapies institute Vector Core, GENETHON Bioexperimentation department and Biogenouest Genomics core facility for their technical assistance. We are also grateful to the AFM sponsored-DMD/µDys network which includes GENETHON, l'Institut de Myologie, Atlantic Gene Therapies and the Royal Holloway (UCL) for providing samples from Golden Retriever muscular dystrophy dogs. This work was performed under a Cooperative Agreement between INSERM, AFM, and the University of Florida Center of Excellence for Regenerative Health Biotechnology. R.S. owns equity in a gene therapy company that is commercializing AAV for gene therapy applications. To the extent that the work in this manuscript increases the value of these commercial holdings, R.S. has a conflict of interest.

REFERENCES

1. Emery, AEH, Muntoni, F and Quinlivan, RCM (2015). *Duchenne Muscular Dystrophy, Fourth edition*, Oxford Monographs on Medical Genetics.
2. Goyenvalle, A, Vulin, A, Fougerousse, F, Leturcq, F, Kaplan, JC, Garcia, L *et al.* (2004). Rescue of dystrophic muscle through U7 snRNA-mediated exon skipping. *Science* **306**: 1796–1799.
3. Foster, H, Sharp, PS, Athanasopoulos, T, Trollet, C, Graham, IR, Foster, K *et al.* (2008). Codon and mRNA sequence optimization of microdystrophin transgenes improves expression and physiological outcome in dystrophic mdx mice following AAV2/8 gene transfer. *Mol Ther* **16**: 1825–1832.
4. Le Guiner, C, Montus, M, Servais, L, Cherel, Y, Francois, V, Thibaud, JL *et al.* (2014). Forelimb treatment in a large cohort of dystrophic dogs supports delivery of a recombinant AAV for exon skipping in Duchenne patients. *Mol Ther* **22**: 1923–1935.
5. Le Hir, M, Goyenvalle, A, Peccate, C, Précigout, G, Davies, KE, Voit, T *et al.* (2013). AAV genome loss from dystrophic mouse muscles during AAV-U7 snRNA-mediated exon-skipping therapy. *Mol Ther* **21**: 1551–1558.
6. Schmidt, WM, Uddin, MH, Dysek, S, Moser-Thier, K, Pirker, C, Höger, H *et al.* (2011). DNA damage, somatic aneuploidy, and malignant sarcoma susceptibility in muscular dystrophies. *PLoS Genet* **7**: e1002042.
7. Colussi, C, Gurtner, A, Rosati, J, Illi, B, Ragone, G, Piaggio, G *et al.* (2009). Nitric oxide deficiency determines global chromatin changes in Duchenne muscular dystrophy. *FASEB J* **23**: 2131–2141.
8. Colussi, C, Mozzetta, C, Gurtner, A, Illi, B, Rosati, J, Straino, S *et al.* (2008). HDAC2 blockade by nitric oxide and histone deacetylase inhibitors reveals a common target in Duchenne muscular dystrophy treatment. *Proc Natl Acad Sci USA* **105**: 19183–19187.
9. Renjini, R, Gayathri, N, Nalini, A and Srinivas Bharath, MM (2012). Oxidative damage in muscular dystrophy correlates with the severity of the pathology: role of glutathione metabolism. *Neurochem Res* **37**: 885–898.
10. Penaud-Budloo, M, Le Guiner, C, Nowrouzi, A, Toromanoff, A, Chérel, Y, Chenuaud, P *et al.* (2008). Adeno-associated virus vector genomes persist as episomal chromatin in primate muscle. *J Virol* **82**: 7875–7885.
11. Léger, A, Le Guiner, C, Nickerson, ML, McGee Im, K, Ferry, N, Moullier, P *et al.* (2011). Adeno-associated viral vector-mediated transgene expression is independent of DNA methylation in primate liver and skeletal muscle. *PLoS One* **6**: e20881.
12. Isken, O and Maquat, LE (2007). Quality control of eukaryotic mRNA: safeguarding cells from abnormal mRNA function. *Genes Dev* **21**: 1833–1856.
13. Schoenberg, DR and Maquat, LE (2012). Regulation of cytoplasmic mRNA decay. *Nat Rev Genet* **13**: 246–259.
14. Canton, M, Menazza, S and Di Lisa, F (2014). Oxidative stress in muscular dystrophy: from generic evidence to specific sources and targets. *J Muscle Res Cell Motil* **35**: 23–36.
15. Rodriguez, MC and Tarnopolsky, MA (2003). Patients with dystrophinopathy show evidence of increased oxidative stress. *Free Radic Biol Med* **34**: 1217–1220.
16. Dudley, RW, Danialou, G, Govindaraju, K, Lands, L, Eidelman, DE and Petrof, BJ (2006). Sarcolemmal damage in dystrophin deficiency is modulated by synergistic interactions between mechanical and oxidative/nitrosative stresses. *Am J Pathol* **168**: 1276–87; quiz 1404.
17. Rivera, VM, Gao, GP, Grant, RL, Schnell, MA, Zoltick, PW, Rozamus, LW *et al.* (2005). Long-term pharmacologically regulated expression of erythropoietin in primates following AAV-mediated gene transfer. *Blood* **105**: 1424–1430.
18. Pacak, CA, Conlon, T, Mah, CS and Byrne, BJ (2008). Relative persistence of AAV serotype 1 vector genomes in dystrophic muscle. *Genet Vaccines Ther* **6**: 14.
19. Cataldi, MP and McCarty, DM (2010). Differential effects of DNA double-strand break repair pathways on single-strand and self-complementary adeno-associated virus vector genomes. *J Virol* **84**: 8673–8682.
20. Cervelli, T, Palacios, JA, Zentilin, L, Mano, M, Schwartz, RA, Weitzman, MD *et al.* (2008). Processing of recombinant AAV genomes occurs in specific nuclear structures that overlap with foci of DNA-damage-response proteins. *J Cell Sci* **121**(Pt 3): 349–357.
21. Lovric, J, Mano, M, Zentilin, L, Eulalio, A, Zacchigna, S and Giacca, M (2012). Terminal differentiation of cardiac and skeletal myocytes induces permissivity to AAV transduction by relieving inhibition imposed by DNA damage response proteins. *Mol Ther* **20**: 2087–2097.
22. Cataldi, MP and McCarty, DM (2013). Hairpin-end conformation of adeno-associated virus genome determines interactions with DNA-repair pathways. *Gene Ther* **20**: 686–693.

© 2015 The American Society of Gene & Cell Therapy

23. Acharyya, S, Sharma, SM, Cheng, AS, Ladner, KJ, He, W, Kline, W *et al.* (2010). TNF inhibits Notch-1 in skeletal muscle cells by Ezh2 and DNA methylation mediated repression: implications in duchenne muscular dystrophy. *PLoS One* **5**: e12479.
24. Ayrapetov, MK, Gursoy-Yuzugullu, O, Xu, C, Xu, Y and Price, BD (2014). DNA double-strand breaks promote methylation of histone H3 on lysine 9 and transient formation of repressive chromatin. *Proc Natl Acad Sci USA* **111**: 9169–9174.
25. Xu, Y, Xu, C and Price, BD (2012). Mechanistic links between ATM and histone methylation codes during DNA repair. *Prog Mol Biol Transl Sci* **110**: 263–288.
26. Tateyama, M, Takeda, A, Onodera, Y, Matsuzaki, M, Hasegawa, T, Nunomura, A *et al.* (2003). Oxidative stress and predominant Abeta42(43) deposition in myopathies with rimmed vacuoles. *Acta Neuropathol* **105**: 581–585.
27. Shan, X, Tashiro, H and Lin, CL (2003). The identification and characterization of oxidized RNAs in Alzheimer's disease. *J Neurosci* **23**: 4913–4921.
28. Poulsen, HE, Specht, E, Broedbaek, K, Henriksen, T, Ellervik, C, Mandrup-Poulsen, T *et al.* (2012). RNA modifications by oxidation: a novel disease mechanism? *Free Radic Biol Med* **52**: 1353–1361.
29. Jacobs, AC, Resendiz, MJ and Greenberg, MM (2010). Direct strand scission from a nucleobase radical in RNA. *J Am Chem Soc* **132**: 3668–3669.
30. Tanaka, M, Chock, PB and Stadtman, ER (2007). Oxidized messenger RNA induces translation errors. *Proc Natl Acad Sci USA* **104**: 66–71.
31. Shan, X, Chang, Y and Lin, CL (2007). Messenger RNA oxidation is an early event preceding cell death and causes reduced protein expression. *FASEB J* **21**: 2753–2764.
32. Görg, B, Qvartskhava, N, Keitel, V, Bidmon, HJ, Selbach, O, Schliess, F *et al.* (2008). Ammonia induces RNA oxidation in cultured astrocytes and brain in vivo. *Hepatology* **48**: 567–579.
33. Chang, Y, Kong, Q, Shan, X, Tian, G, Ilieva, H, Cleveland, DW *et al.* (2008). Messenger RNA oxidation occurs early in disease pathogenesis and promotes motor neuron degeneration in ALS. *PLoS One* **3**: e2849.
34. Bustin, SA, Benes, V, Garson, JA, Hellemans, J, Huggett, J, Kubista, M *et al.* (2009). The MIQE guidelines: minimum information for publication of quantitative real-time PCR experiments. *Clin Chem* **55**: 611–622.
35. Pfaffl, MW. A new mathematical model for relative quantification in real-time RT-PCR. (2001). *Nucleic Acids Res* **29**: e45.

This work is licensed. under a Creative Commons Attribution-NonCommercial-ShareAlike 4.0 International License. The images or other third party material in this article are included in the article's Creative Commons license, unless indicated otherwise in the credit line; if the material is not included under the Creative Commons license, users will need to obtain permission from the license holder to reproduce the material. To view a copy of this license, visit http://creativecommons.org/licenses/by-nc-sa/4.0/

Supplementary Information accompanies this paper on the *Molecular Therapy—Methods & Clinical Development* website (http://www.nature.com/mtm)